Seismic bearing capacity of shallow foundations on soil reinforced by rigid inclusions

Y Shen, J Pérez-Herreros, F Cuira, S Burlon, J-F Semblat

Proceedings of the XVIII ECSMGE 2024
GEOTECHNICAL ENGINEERING CHALLENGES
TO MEET CURRENT AND EMERGING NEEDS OF SOCIETY

ISBN 978-1-032-54816-6
DOI 10.1201/9781003431749-371

ECSMGE 24
XVIII EUROPEAN CONFERENCE ON SOIL MECHANICS AND GEOTECHNICAL ENGINEERING

Seismic bearing capacity of shallow foundations on soil reinforced by rigid inclusions

Capacité portante sismique des fondations sur sol renforcé par inclusions rigides

Y. Shen*
IMSIA (UMR 9219), CNRS, EDF, CEA, ENSTA Paris, Institut Polytechnique de Paris, Palaiseau, France / TERRASOL (SETEC Group), Paris, France

J. Pérez-Herreros, F. Cuira, S. Burlon
TERRASOL (SETEC Group), Paris, France

J-F. Semblat
IMSIA (UMR 9219), CNRS, EDF, CEA, ENSTA Paris, Institut Polytechnique de Paris, Palaiseau, France

**yuxiang.shen@setec.com*

ABSTRACT: The kinematic exterior approach, in the framework of the yield design theory, is widely utilised for assessing foundation bearing capacity. This study aims at extending this approach to shallow foundations on reinforced soil by rigid inclusions. The interaction diagram in the (V, H, M) space is obtained by combining the interaction curves derived from different failure mechanisms. The resisting forces provided by the rigid inclusions are evaluated using a multicriterion approach and are considered at the intersection of the inclusions with the failure surface. Furthermore, the soil inertia due to the horizontal seismic excitation is also considered in the analysis. The results reveal that the bearing capacity under seismic load is unaffected in the zone of interest for foundations with a sufficient safety factor under static loading.

RÉSUMÉ: L'approche cinématique par l'extérieur, dans le cadre de la théorie de calcul à la rupture, est largement utilisée pour évaluer la capacité portante des fondations. Cette étude vise à étendre cette approche aux fondations renforcées par inclusions rigides. Pour ce faire, le diagramme d'interaction dans l'espace (H, V, M) est obtenu en combinant les diagrammes d'interaction issus de différents mécanismes de rupture. L'effet de renforcement apporté par les inclusions rigides est pris en compte au moyen des forces résistantes développées à l'intersection de l'inclusion avec la surface de rupture, et sont évaluées à l'aide d'un multicritère. De plus, cette étude prend en compte les effets d'inertie du. Les résultats révèlent que la capacité portante sous charge sismique n'est pas impactée dans la zone d'intérêt pour les fondations présentant un facteur de sécurité suffisant sous charge statique.

Keywords: Yield design; bearing capacity; rigid inclusion-reinforced foundation; ASIRI+.

1 INTRODUCTION

The reinforcement technique using rigid inclusions (RI), represents an alternative foundation solution that offers significant technical and economic advantages in comparison to conventional pile foundations. This technique has been used successfully in numerous projects involving complicated geotechnical contexts.

This foundation concept consists of a shallow foundation on a reinforced soil with vertical rigid elements, known as rigid inclusions, which reduce the foundation settlement while enhancing its vertical bearing capacity. There is no direct connection between the shallow foundation and the RIs. Instead, a gravel layer is introduced as a load transfer platform (LTP) as depicted in Figure 1.

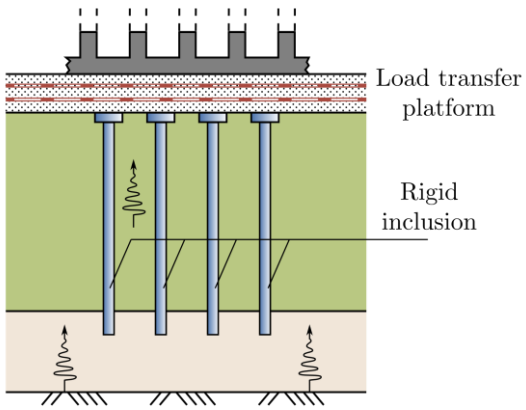

Figure 1. Shallow foundation on soil reinforced by rigid inclusions under seismic loading.

Recent studies have focussed on the dynamic response of such foundations (Shen et al., 2022a, b,

2023). However, the question of the bearing capacity under static and seismic loading has not yet been studied in detail and no practical methodology is available. Consequently, this study focuses on addressing the seismic bearing capacity problem of RI-reinforced foundations using the kinematic exterior approach.

2 KINEMATIC EXTERIOR APPROACH

2.1 Theoretical framework

Within the context of the yield design theory, the kinematic exterior approach operates as an upper-bound analysis method. This approach involves evaluating a kinematically admissible virtual velocity field $\underline{\hat{U}}$ and verifying whether the virtual power of external loads applied to the system, denoted as P_e, is less than or equal to the maximum resisting power of the soil, denoted as P_{rm}.

An upper-bound K encompasses the space delineated by:

$$K \subset \{P_{rm}(\underline{\hat{U}}) \geq P_e(\underline{\hat{U}})\} \quad (1)$$

The maximum resisting power P_{rm} is equal to:

$$P_{rm}(\underline{U}) = \int_\Omega \pi\left(\underline{\hat{d}}\right) d\Omega + \int_\Sigma \pi(\llbracket \underline{\hat{U}} \rrbracket)\, d\Sigma \quad (2)$$

where $\pi(.)$ represents the density of virtual power due to the strain rate $\underline{\hat{d}}$ within the volume Ω and to the virtual velocity $\llbracket \underline{\hat{U}} \rrbracket$ at the velocity discontinuity surface Σ. These quantities are derived from the strength criteria. The explicit formulation of the function $\pi(.)$ for various criteria, applicable to both continuous materials and interfaces, can be found in the work of Salençon (1983, 2002).

The virtual power of all external forces P_e applied to the system encompasses the power of the loads exerted on the foundation, in terms of forces and moments, as well as the body forces originating from soil inertia.

In the case of a foundation reinforced by RIs, the formulation of P_e remains unchanged when compared to the case without reinforcement. Nonetheless, the contribution of reinforcement by RIs, represented by P_{RIs}, should be added into the resisting power part, as outlined in:

$$K \subset \{P_{rm}(\underline{\hat{U}}) + P_{RIs}(\underline{\hat{U}}) \geq P_e(\underline{\hat{U}})\} \quad (3)$$

2.2 Application to the study of geotechnical structures

The kinematic exterior approach has been employed in previous work to investigate the bearing capacity of strip foundations resting on homogeneous cohesive and cohesionless soils subjected to static and seismic loads (Salençon and Pecker, 1995a, 1995b; Paolucci and Pecker, 1997; Soubra, 1999).

It can be also found that the kinematic exterior approach has already been used to study the stability problem of reinforced geotechnical structures, such as nailed slopes.

De Buhan et al. (1992) investigated the stability of nailed slopes using the kinematic exterior approach. The study comprised kinematic mechanisms based on triangular blocks and logarithmic spiral failure surfaces. Several slope stability softwares, including TALREN (Terrasol, 2023), PROSPER (De Sauvage and Rajot, 2018), and STARS (Antoine, 1990), also employ failure surfaces in the form of logarithmic spirals. The contribution of nail reinforcements is introduced by employing a multicriterion approach based on various failure modes associated with the nails.

Very few applications of the kinematic exterior approach to study RI-reinforced foundations have been conducted so far. This is partly due to the inherent complexity introduced by the presence of the three distinct components: the soft soil, the granular LTP, and the RIs, which makes it difficult to determine kinematically admissible virtual velocity fields $\underline{\hat{U}}$.

Pecker et al. (1998) evaluated the seismic bearing capacity of a shallow foundation on cohesive soil reinforced by RIs, using the kinematic exterior approach. The findings were compared with the results of five centrifuge tests carried out for the Rio-Antirrio bridge project. Figure 2 presents a kinematic mechanism considered in that study, which closely resembles the failure mechanism observed in the centrifuge tests.

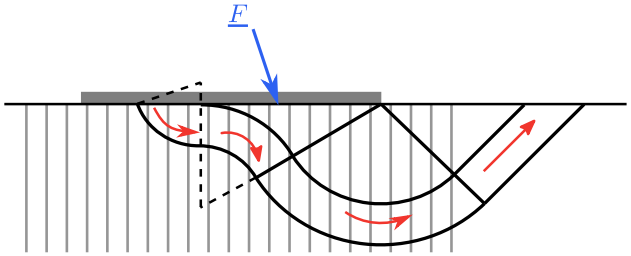

Figure 2. Virtual velocity field considered in the bearing capacity estimation of the Rio-Antirrio bridge foundation.

In this mechanism, the contribution of the RIs was considered by the intrinsic material resistance and their skin friction. Additionally, a failure criterion

representing the slide failure between the LTP and the foundation was introduced and superimposed onto the results obtained through the kinematic exterior approach.

3 BEARING CAPACITY OF A STRIP FOOTING ON REINFORCED SOIL

3.1 Description of the problem

This study focuses on the seismic bearing capacity of a strip foundation on reinforced soil by RIs. A strip foundation of width B is placed on a half-space consisting of a LTP of thickness h_{LTP} and purely cohesionless behaviour (friction angle φ), over a cohesive soft soil layer with a cohesion c and no tensile strength. The soft soil layer is reinforced with RIs, as illustrated in Figure 3.

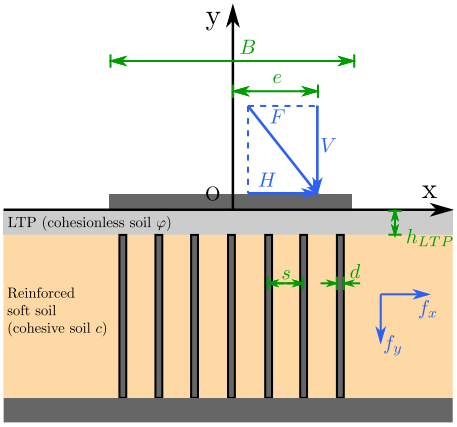

Figure 3. Studied configuration: strip foundation on reinforced soil by Ris.

The RI rows are modelled by embedded beams. They are assumed to be regularly spaced under the foundation with a spacing s and are embedded in the compact soil layer.

The force transmitted to the footing is denoted as $\underline{F}$, and the moment $\underline{M}$ is calculated by multiplying the vertical force by the eccentricity e.

Additionally, the soil inertia effects are considered through body forces due to seismic and gravity loading, denoted as $f_x = \rho a_x$ and $f_y = \rho(g \pm a_y)$, respectively. The horizontal

3.2 Simplified sub-systems

The presence of reinforcements and the LTP layer in RI-reinforced foundations introduces additional complexity to the failure mechanisms when compared to non-reinforced configurations. To address this, three simplified sub-systems (or cases), illustrated in Figure 5, are proposed, corresponding to the different potential failure mechanisms are investigated:

- Case I: This sub-system considers a homogeneous frictional soil, where the failure mechanism is primarily concentrated in the LTP, resulting in a failure depth lower than h_{LTP};
- Case II: This sub-system deals with the potential sliding and uplift at the interface between the LTP and the reinforced soft soil;
- Case III: Involves a homogeneous cohesive soil reinforced by RIs. The failure mechanism depth in this case exceeds h_{LTP} and intersects the RIs, that contribute thus to the resistance. It should be noted that the contribution of the soil and the RIs are calculated separately, as depicted in Figure 6.

The upper-bound solutions for the three cases are denoted $K^{up,I}$, $K^{up,II}$, and $K^{up,III}$. They are combined to determine the stability domain K^{up} of a foundation reinforced by RIs, as described in :

$$K^{up} = K^{up,I} \cap K^{up,II} \cap K^{up,III} \quad (4)$$

3.3 Failure analysis of a rigid inclusion

The RIs are considered by accounting for their action at the intersection with the failure surface. The RI is divided into two parts by the intersection: interior part with a length L_{int} and exterior part with length L_{ext}, as depicted in Figure 4 (a). The forces at this intersection are decomposed into an axial force T_n, a shear force T_c, and a bending moment M_c, as shown in Figure 4 (b). Their maximum value are limited by several criteria:

- Material intrinsic strength;
- Vertical interaction resistance;
- Lateral interaction resistance: plastification of the soil;
- Lateral interaction resistance: plastification of the RI.

3.3.1 Material intrinsic strength resistance

The combination of T_n, T_c, and M_c that occurs at the intersection of the RIs with the velocity discontinuity surface can be represented by:

$$\left(\frac{T_n}{R_n}\right)^2 + \left(\frac{T_c}{R_c}\right)^2 + \left|\frac{M_c}{R_m}\right| - 1 \leq 0 \quad (5)$$

where R_n, R_c, and R_m are the axial, shear, and flexural capacities of a rigid inclusion related to the material intrinsic strength and the inclusion's section. In the case with the presence of the steel reinforcement in the concrete inclusions, the reinforcement should be considered.

3.3.2 Axial soil-inclusion interaction resistance

The maximum axial force T_{nl} that a RI of diameter d can provide is also governed by parameters such as the skin friction, the forces at the head and the tip of the RI, and the internal "pullout" failure mechanism. This can be described by:

$$T_{nl} = min\,(F_0 + q_s L_{int}\pi d, F_L + q_s L_{ext}\pi d) \quad (6)$$

where F_0 represents the maximum force controlled by a Prandtl failure mechanism in the LTP, F_L represents the maximum force at the inclusion tip, which is typically of significant magnitude. Additionally, q_s denotes the characteristic value of the inclusion shaft friction.

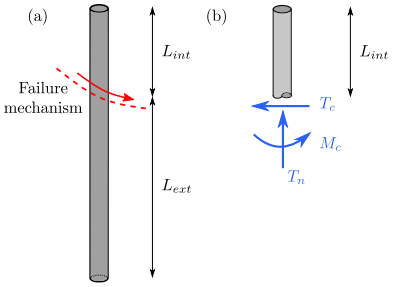

Figure 4. Scheme of a RI intersected by a failure mechanism: (a) interior length L_{int} and exterior length L_{ext} and (b) RI forces at the intersection.

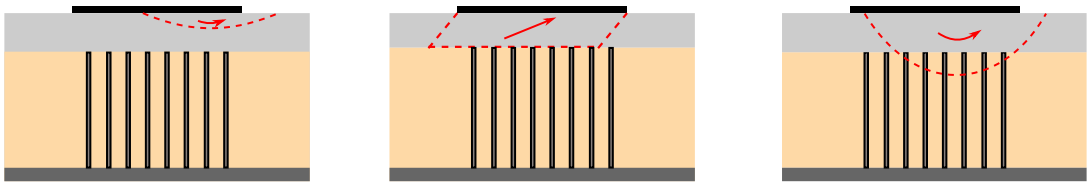

Figure 5. Simplified sub-systems for a foundation reinforced by Ris.

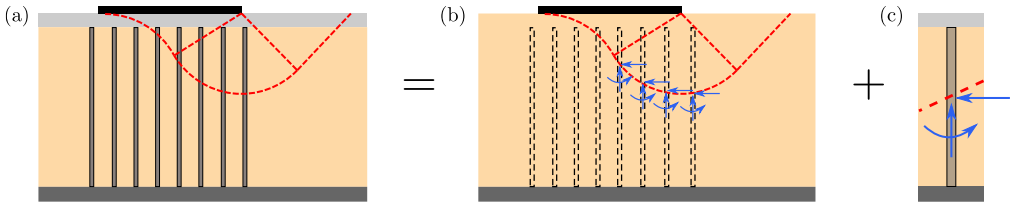

Figure 6. Detailed description for Case III: (a) multi-block failure mechanism, (b) simplified configuration, and (c) forces at the intersection of RI with failure interaction.

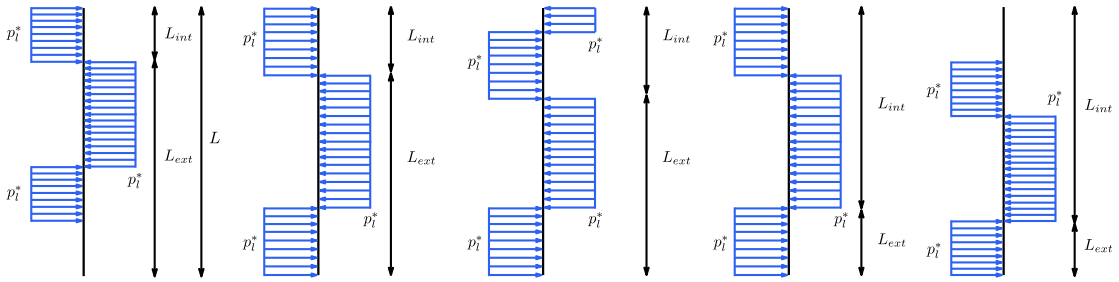

(a) $L_{int} < L/4$ (b) $L_{int} = L/4$ (c) $L/4 < L_{int} < 3L/4$ (d) $L_{int} = 3L/4$ (e) $L_{int} > 3L/4$

Figure 7. Distribution of lateral pressure for limit equilibrium model.

3.3.3 Lateral soil-inclusion interaction resistance

This criterion corresponds to the mobilised resistance due to lateral soil-inclusion interaction. The pressure within the interior length L_{int} or the exterior length L_{ext} of the RI is restricted by the limit pressure p_l^* in the soil.

The lateral interaction of the RI is analysed through a limit equilibrium model, as depicted in Figure 7. Several lateral pressure distributions for various lengths L_{int} and L_{ext} are considered.

The corresponding shear force T_{cl1} and bending moment M_{cl} at the intersection and the maximum bending moment M_{max} within the RI generated by the lateral pressure can be expressed with respect to the ratio L_{int}/L, as shown in Figure 8.

3.3.4 Formulation of the RI multicriterion

The combination of the four criteria in the T_n-T_c plane defines a useful stability domain, known as the RI multicriterion and illustrated in Figure 9. This domain

establishes the limits on the potential resisting forces provided by the RIs.

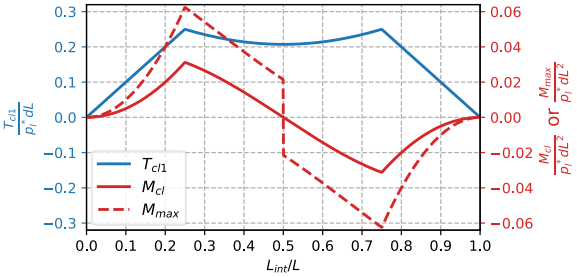

Figure 8. Evaluation of T_{cl1}, M_{cl}, and M_{max} due to soil-inclusion lateral interaction for different values of the ratio L_{int}/L.

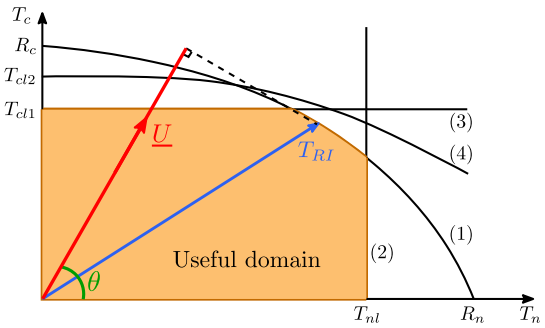

Figure 9. RI multicriterion in the T_n-T_c plane.

When failure occurs, the resisting forces developed by the RI must lie on the boundary of this useful domain, and its position is determined by the principle of maximum work. This principle indicates that the forces on the boundary are chosen in a way that maximises the resisting power provided by rigid inclusions within a given failure mechanism. Once the virtual velocity at the intersection of the inclusion with the failure surface is specified, the virtual power of the inclusion can be calculated.

3.4 Practical application

A typical foundation configuration is considered. It consists of a 10 m wide strip foundation, resting on a 0.5 m thick LTP layer with a friction angle of 38°. The soft soil is considered as cohesive, characterised by an undrained shear strength c of 25 kPa, a q_s = 25 kPa and p_l^* = 200 kPa. The soft soil is reinforced by rows of RI with a diameter of 0.4 m and a length of 10 m. The axis-to-axis spacing is 1.5 m, resulting in a coverage area ratio of 5.6 %. The head of the RI corresponds to the base of the LTP.

The bearing capacity of the foundation is studied using the approach presented in the previous sections. The interaction diagram is normalised by the product of the cohesion c and the width of the foundation B, as depicted in Figure 10.

For small vertical forces, the V-H interaction diagram is predominantly controlled by Case I (blue curve), corresponding to failure within the LTP layer. As the vertical force increases, a sliding mechanism between the LTP and the soft soil becomes apparent (green curve). Finally, for greater vertical forces, the interaction diagram is primarily controlled by Case III (red curve), which represents a failure mechanism in the reinforced soil.

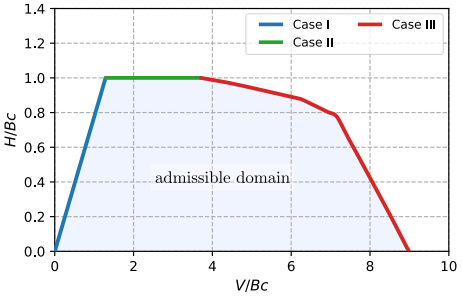

Figure 10. Bearing capacity of a strip foundation on reinforced soil by RI in the normalised V-H plane.

4 SOIL INERTIA EFFECT ON THE BEARING CAPACITY

4.1 Interaction diagram under various soil inertia values

The adverse impact of soil inertia forces on the bearing capacity of non-reinforced foundations can be significant, particularly for foundations designed with a low safety factor under a vertical centred load. This impact for RI-reinforced foundations is studied in this section.

The V-H interaction curves for several acceleration values in the soil ranging from 0 to 0.4 g are displayed in Figure 11.

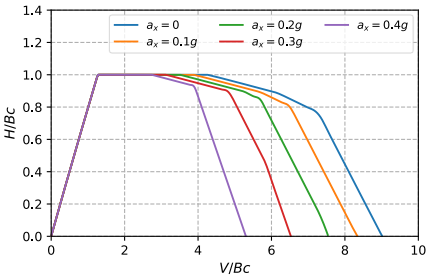

Figure 11. Normalised V-H interaction curves for different ground accelerations.

It is observed that the shape of the V-H interaction curves is not affected by soil inertia effects, and only the amplitude of their right-hand side (Case III), which is controlled by the failure mechanism traversing the reinforced soil, is influenced by the soil inertia.

4.2 Bearing capacity under different soil inertia values

The bearing capacity, denoted V_{max}, represents the maximum vertical centred force that a foundation can carry. Figure 12 explores the bearing capacity values with different soil inertia values due to the horizontal seismic excitation. The soil inertia values are represented by the dimensionless soil inertia forces $\bar{F} = \rho a_x B/c$. Comparing the non-reinforced configuration (orange curve) to the reinforced configurations (blue curves for different coverage area ratios α), it can be observed that the rigid inclusion improvement enhances the foundation bearing capacity V_{max} to withstand the soil inertia.

For example, at a dimensionless soil inertia force of $\bar{F} = 2$, corresponding to a situation with $a_x = 0.33$ g, $\rho = 1.8\ t/m^3$, $B = 10\ m$, and $c = 25\ kPa$, the non-reinforced foundation exhibits a 50 % reduction in its bearing capacity due to soil inertia effect. In contrast, the reinforced configuration with the same soil inertia still retains approximately 80 % of its bearing capacity.

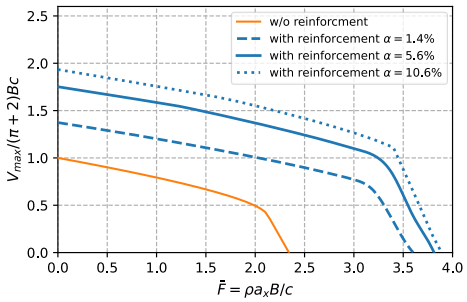

Figure 12. Evolution of the bearing capacity V_{max} of the foundation with respect to different soil inertia values.

5 CONCLUSIONS

This work extends the application of the kinematic exterior approach to rigid inclusion-reinforced foundations. To accurately estimate the contribution of the inclusions to the resistance of the system.

The bearing capacity under the soil inertia is studied for reinforced configurations with different coverage area ratios, revealing that the bearing capacity consistently increases as the coverage area ratio does. The interaction diagrams reveal that the bearing capacity under seismic load is unaffected in the zone of interest for foundations with a sufficient safety factor under static loading.

ACKNOWLEDGEMENTS

The authors are grateful for the financial support provided by Terrasol company. This research has received funding from the French National Research (ANR) project ASIRI_plus SDS reference No. ANR-19-CE22-0015-01.

REFERENCES

Anthoine, A. (1987). Stabilité d'une fouille renforcée par clouage. In: *Proc. 4th French-Polish Coll. appl. Soil Mech.*, Grenoble, France, pp. 129-154.

De Buhan, P., Dormieux, L. and Salençon, J. (1992). An interactive computer software for the yield design of reinforced soil structures. In *Coll. Informatique et Géotechnique,* Paris, France, pp. 181-188.

De Sauvage, J. and Rajot, J. P. (2018). Clouage des sols: conditions de long terme et amélioration du dimensionnement conventionnel. In *9emes JNGG.* Champs sur Marne, France

Paolucci, R. and Pecker, A. (1997). Seismic bearing capacity of shallow strip foundations on dry soils. *Soils Found.*, 37(3), pp. 95-105. https://doi.org/10.3208/sandf.37.3_95

Pecker, A., Harikiopoulos, H., de Buhan, P., Dormieux, L., Morand, P. (1998). Comportement sismique d'une fondation sur sol renforcé par inclusions rigides, Paris, France. Compte rendu pour MRES.

Salençon, J. (1983). *Calcul à la rupture et analyse limite*, Presses de l'École Nationale des Ponts et Chaussées, Paris, France.

Salençon, J. (2002). *De l'élasto-plasticité au calcul à la rupture*. Editions Ecole Polytechnique, Paris, France.

Salençon, J. and Pecker, A. (1995a). Ultimate bearing capacity of shallow foundations under inclined and eccentric loads. Part I: purely cohesive soil. *European journal of mechanics series a solids*, 14, pp. 349-349.

Salençon, J. and Pecker, A. (1995b). Ultimate bearing capacity of shallow foundations under inclined and eccentric loads. Part II: purely cohesive soil without tensile strength. *European journal of mechanics series a solids*, 14, pp. 377–96.

Shen, Y., Pérez-Herreros, J., Cuira, F., Semblat, J. F. and Burlon, S. (2022a). Interaction inertielle sol-structure d'un massif renforcé par inclusions rigides. In *11èmes JNGG*, Lyon, France.

Shen, Y., Pérez-Herreros, J., Cuira, F., Semblat, J. F. and Burlon, S. (2022b). Interaction cinématique sol-structure d'un massif renforcé par inclusions rigides sous séisme. In *11èmes JNGG*, Lyon, France.

Shen, Y., Pérez-Herreros, J., Cuira, F., Semblat, J. F. and Burlon, S. (2023). Evaluation des efforts d'origine inertielle dans les inclusions rigides. In *11ème Colloque National de l'AFPS*, Guadeloupe, France.

Soubra, A. H. (1999). Upper-bound solutions for bearing capacity of foundations. *J. Geotech. Geoenvironmental Eng.*, 125(1), pp. 59-68. https://doi.org/10.1061/(ASCE)1090-0241(1999)125:1(59)

Terrasol (2023) TALREN (v6): Advanced slope stability analysis with or without reinforcements, [Computer software].